Accuracy and performance of fluid-structure interaction algorithms with explicit versus implicit formulations of the fluid solver

YiQin Xu* and Yulia Peet†

School for Engineering of Matter, Transport and Energy, Arizona State University

Fluid structure interaction (FSI) describes a problem when a solid structure deforms or oscillates by the influence of the fluid flow, and thus a two-way interaction occur, such as in wind turbines, airfoils, parachutes, biological systems, including aneurysms, etc. One of the major challenges in the numerical simulation of this problem is the computational cost, and most of the current solvers are using an implicit method for fluid, with Newton-Raphson method being the most popular. However, an explicit method is relatively cheap. In this paper, explicit method with sub-iterations is compared with a Newton-Raphson method through an FSI benchmark case. We concentrate on comparison of accuracy as well as the computational performance of the two methods.

I. Introduction

Fluid-structure interaction is a multi-physics problem since it is dependent on both fluid and structure behaviour, and their interaction. Numerical integration of such coupled systems has traditionally relied on two main approaches, monolithic coupling[1–6] and partitioned coupling.[7–10] Monolithic coupling is when both fluid and solid equations are solved in one system. This method is capable of providing high accuracy for the fluid-structure interaction behavior. However, such method requires a new solver and the resulting system is very large and difficult to solve. To reuse the existing solvers, partitioned coupling could be used when the fluid and solid equations are solved iteratively. Separate fluid and solid solvers would be run sequentially with only the boundary conditions needed to be transferred to satisfy the continuity laws. These methods are unfortunately known to converge slower, and added-mass instability[10] for high density ratios may occur.

To couple non-linear fluid and solid equations in a monolithic way, most of the FSI papers are using implicit `Newton-Raphson` method.[5,6,11,12] Moreover, even when a partitioned coupling is performed, to resolve the non-linearities in the fluid, the `Newton-Raphson` method is often used as well.[5,6,11,12] However, `Newton-Raphson` method is difficult to implement, and it might increase the computational costs compared to explicit method. Then the question arises whether it is necessary to have an implicit method for fluid with partitioned coupling for the FSI problem? To answer that question, a comparison is performed between an explicit method with sub-iterations and a fully implicit scheme based on `Newton-Raphson` method in a partitioned coupling framework, through FSI benchmark in this paper.

II. Numerical Method

Spectral element method implemented in the code Nek5000[13,14] is used for all of the simulations we introduce here. It is similar in the form to finite-element methods[15] but the basis functions are high-order polynomials associated with Gauss-Lobatto points which helps leverage the tensor-product efficiency and obtain fast convergence. Fluid structure interaction is implemented by a partitioned coupling technique[7] with Aitken relaxation method. It only requires the communication of the boundary conditions which transfer stress or traction from fluid to solid, and velocity from solid to fluid on the interface. For the purpose of comparing with the FSI benchmark,[16] the solid part is using `St. Venant-Kirchhoff` nonlinear constitutive

*Ph.D. student, AIAA member, e-mail: yiqinxu@asu.edu

†Assistant Professor, AIAA member, e-mail: ypeet@asu.edu

law material. The fluid part in our formulation is governed by the incompressible flow equations and is solved using an `Arbitrary Lagrangian-Eulerian` (ALE)[5,17] framework. In this paper, it will be solved either by a semi-explicit scheme[14] with a sub-iteration method[18] or by an implicit `Newton-Raphson` method.[5,19]

II.A. Explicit scheme, backward difference with extrapolation

The strong form of the Navier-Stokes equations with the incompressibility constraint in the ALE formulation is

$$\rho(\frac{\partial u}{\partial t}\Big|_{\hat{x}} + (u-\hat{u})\cdot\nabla u - f) + \nabla p - \mu\Delta u = 0, \tag{1}$$

$$\nabla\cdot u = 0, \tag{2}$$

where ρ, u, f, p, μ and $\hat{u}$ are the fluid density, velocity, external force, pressure, dynamic viscosity and mesh velocity, respectively. Besides, the $\frac{\partial}{\partial t}\Big|_{\hat{x}}$ denotes the time derivative when the reference fluid domain is fixed. The difficulty in solving such a system is the non linearity of the convective term, and a very common way to overcome it is to use an explicit extrapolation from previous time steps. As implemented before, Nek5000 was using backward difference for time discretization, and extrapolation for the nonlinear term. The linear diffusion term would be treated implicitly, so the velocity could be solved via a Helmholtz equation,

$$\frac{\beta_k\bar{u}}{\delta t} - \frac{\mu}{\rho}\Delta\bar{u} = -\sum_{j=1}^{k}\frac{\beta_{k-j}}{\delta t}u^{n+1-j} - \sum_{j=1}^{k}\alpha_j[(u-\hat{u})\cdot\nabla u]^{n+1-j} - \frac{\nabla\bar{p}^{n+1}}{\rho} + f^{n+1}. \tag{3}$$

The superscript in Eq. (3) denotes the time step, and velocity and pressure of the time step $n+1$ are unknown. Coefficients β and α represent the coefficients of the backward difference and the extrapolation of a certain order k. The variables with a bar, $\bar{u}$, $\bar{p}^{n+1} = 2p^n - p^{n-1}$, are the intermediate velocity and extrapolated pressure, which are further updated as

$$\Delta(p^{n+1} - \bar{p}^{n+1}) = \nabla\cdot(\frac{\beta_k\bar{u}}{\delta t}), \tag{4}$$

$$u^{n+1} = \bar{u} - \frac{\delta t}{\beta_k}\nabla\cdot(p^{n+1} - \bar{p}^{n+1}), \tag{5}$$

to arrive at a final velocity and pressure at each time step. This method is usually used for a staggered mesh to satisfy inf-sup condition,[14,20] and it is called $P_N - P_{N-2}$.[14]

The advantage of such a scheme is the effectiveness and the speed. Helmholtz equation for velocity could be solved efficiently either by Preconditioned Conjugate Gradient (`PCG`) or Generalized Minimal Residual Method (`GMRES`) with the inverse of diagonal preconditioning. The Poisson equation for pressure could be solved by `GMRES` with multi-grid preconditioning.[14] Once the velocity and pressure fields very slowly in time, and the time step δt is picked adequately, this scheme can have accurate results on stationary and moving meshes.[21] However, in the problems with abrupt, or impulsive motions, be it a sudden change in the inflow flux, or a sudden motion of a solid boundary, the explicit extrapolation of the convective term causes a strong mismatch between the new, implicit value, and an extrapolated value, that is reflected in a sporadic pressure behaviour and subsequent numerical instabilities. Unfortunately, this is an issue for the FSI problem since the mesh motion can vary rapidly in time and can no longer be predicted easily by extrapolation.

II.B. Semi-explicit scheme, sub-iteration method

One approach to overcome this limitation, suggested by Karniadakis's group,[18,22,23] is to use sub-iteration method to have converged velocity and pressure fields which imitate an implicit scheme. The main idea is that, after solving Eqs. (3, 4, 5), the results are treated as some intermediate values v_1^{n+1} and p_1^{n+1} and are substituted back into Eqs. (3, 4, 5) to arrive at the next approximation, v_2^{n+1} and p_2^{n+1},

$$\frac{\beta_k\bar{u}}{\delta t} - \frac{\mu}{\rho}\Delta\bar{u} = -\sum_{j=1}^{k}\frac{\beta_{k-j}}{\delta t}u^{n+1-j} - [(u_1^{n+1}-\hat{u})\cdot\nabla u_1^{n+1}] - \frac{\nabla p_1^{n+1}}{\rho} + f^{n+1}, \tag{6}$$

$$\Delta(p_2^{n+1} - p_1^{n+1}) = \nabla \cdot (\frac{\beta_k \bar{u}}{\delta t}), \tag{7}$$

$$u_2^{n+1} = \bar{u} - \frac{\delta t}{\beta_k} \nabla \cdot (p_2^{n+1} - p_1^{n+1}). \tag{8}$$

The procedure is then repeated iteratively until normalized L-2 error norm $\frac{|u_{i+1}^{n+1} - u_i^{n+1}|_2}{|u_i^{n+1}|_2}$, and $\frac{|p_{i+1}^{n+1} - p_i^{n+1}|_2}{|p_i^{n+1}|_2}$ converge to a certain tolerance. As needs to be mentioned, here the order of the backward difference scheme k will be limited to the first or second order for stability.[18]

With such method, the fluid solver could avoid the mismatch problem for extrapolated convective term mentioned in Sec. (II.A) and give converged results. The iteration converges fast and could also increase the Courant number limit.[18]

II.C. Implicit scheme, Newton-Raphson method

For a fully implicit treatment of the nonlinear convective term, Newton-Raphson method is commonly used.[5,6,11,12] In this method, a linearization of the convective term is performed, and Eqs. (1, 2) are solved iteratively. To begin with, the weak form of Eqs. (1, 2) is stated as: find $u \in H_0^1(\Omega)^d$ and $p \in L_0^2(\Omega)$ such that $\forall w \in H_0^1(\Omega)^d$ and $\forall q \in L_0^2(\Omega)$.

$$\int_{\Omega_t} w \cdot \rho(\frac{\partial u}{\partial t}\bigg|_{\hat{x}} + (u - \hat{u}) \cdot \nabla u - f)\, d\Omega + \int_{\Omega_t} w \cdot \nabla p\, d\Omega - \int_{\Gamma_t} w \cdot (\mu \nabla u) n\, d\Gamma + \int_{\Omega_t} \mu \nabla w : \nabla u\, d\Omega = 0, \tag{9}$$

$$\int_{\Gamma_t} q(u) n\, d\Gamma - \int_{\Omega_t} \nabla q \cdot u\, d\Omega = 0. \tag{10}$$

Here $H_0^1(\Omega_t)^d$ denotes the Sobolev space of vector functions with d components, vanishing to zero on a Dirichlet boundary, and $L_0^2(\Omega_t)$ denotes the Hilbert space of vector functions that are square-integrable and have a zero mean value over the essential (pressure) boundary.

The integration domain Ω_t is chosen as the current fluid domain at time step $n+1$, and the mesh velocity $\hat{u}^{n+1}$ can be computed from an elastic equation,[5] with the prescribed boundary condition and modified Young's modulus and Poisson's ratio. Upon which, the Newmark formula[19] can be used for the time discretization with $\gamma = 0.5$:

$$u^{n+1} = u^n + \delta t[(1-\gamma)\dot{u}^n + \gamma \dot{u}^{n+1}], \tag{11}$$

where $\dot{u}$ denotes the partial derivative of u with respect to time. Newton-Raphson method would then have a prediction and multi-correction steps in the algorithm. At time step $n+1$, an initial solution would be given as

$$\begin{aligned} \dot{u}_1^{n+1} &= (\frac{\gamma - 1}{\gamma})\dot{u}^n, \\ u_1^{n+1} &= u^n, \\ p_1^{n+1} &= p^n. \end{aligned} \tag{12}$$

Then, the increment of acceleration and pressure would be solved by

$$\begin{aligned} \frac{\partial N_M}{\partial \dot{u}^{n+1}}\bigg|_i \delta \dot{u}_i^{n+1} + \frac{\partial N_M}{\partial p^{n+1}}\bigg|_i \delta p_i^{n+1} &= -N_M\Big|_i, \\ \frac{\partial N_C}{\partial \dot{u}^{n+1}}\bigg|_i \delta \dot{u}_i^{n+1} + \frac{\partial N_C}{\partial p^{n+1}}\bigg|_i \delta p_i^{n+1} &= -N_C\Big|_i, \end{aligned} \tag{13}$$

where $N_M\Big|_i$ and $N_C\Big|_i$ are the discretized residuals in the Eq. (9) and Eq. (10) with the unknowns at ith iteration. The gradient matrix such as $\frac{\partial N_M}{\partial \dot{u}^{n+1}}$ can be solved from

$$\frac{\partial N_M}{\partial \dot{u}^{n+1}}\bigg|_i \delta \dot{u}_i^{n+1} = \frac{d}{d\omega} N_M(\dot{u}^{n+1} + \omega \delta \dot{u}_i^{n+1})\bigg|_{\omega=0,\ at\ i} \tag{14}$$

To cast Eq. (13) into the matrix form and to simplify the notation, the system that needs to be solved is

$$\begin{bmatrix} F & G \\ D & 0 \end{bmatrix} \begin{bmatrix} \delta u_i^{n+1} \\ \delta p_i^{n+1} \end{bmatrix} = \begin{bmatrix} -f \\ -g \end{bmatrix}, \tag{15}$$

with a simpler notation F, G, D, f, g standing for $\frac{\partial N_M}{\partial \dot{u}^{n+1}}$, $\frac{\partial N_M}{\partial p^{n+1}}$, $\frac{\partial N_C}{\partial \dot{u}^{n+1}}$, $N_M\Big|_i$ and $N_C\Big|_i$. However, it is not straightforward to solve such system directly. An inexact LU factorization Yosida-2 algorithm[24–26] is implemented to solve Eq. (15) here. The employed inexact factorization algorithm first recognizes an exact identity

$$\begin{bmatrix} F & G \\ D & 0 \end{bmatrix} = \begin{bmatrix} F & 0 \\ D & -DF^{-1}G \end{bmatrix} \begin{bmatrix} I & F^{-1}G \\ 0 & I \end{bmatrix}, \tag{16}$$

which is then approximated by using M^{-1} instead of F^{-1}, where M^{-1} is the inverse of the mass matrix. As needs to be mentioned, the mass matrix in a spectral element method is purely diagonal. Then, the procedure can be generalized with three equations:

$$F\ \delta\tilde{\dot{u}}_i^{n+1} = -f, \tag{17}$$

$$DM^{-1}G\ \delta p_i^{n+1} = g + D\ \delta\tilde{\dot{u}}_i^{n+1}, \tag{18}$$

$$F\ \delta\dot{u}_i^{n+1} = F\ \delta\tilde{\dot{u}}_i^{n+1} - G\ \delta p_i^{n+1}. \tag{19}$$

The limitation on the time step δt is necessary here due to stability in solving Eqs. (17, 19). Multi-grid preconditioning is used for solving Eq. (18) with `GMRES`. The last step of a multi-correction is updating the solution as

$$\begin{aligned} \dot{u}_{i+1}^{n+1} &= \dot{u}_i^{n+1} + \delta\dot{u}_i^{n+1}, \\ u_{i+1}^{n+1} &= u_i^{n+1} + \delta t\gamma\delta u_i^{n+1}, \\ p_{i+1}^{n+1} &= p_i^{n+1} + \delta p_i^{n+1}. \end{aligned} \tag{20}$$

The iterations end when the normalized L-2 error norm $\frac{|u_{i+1}^{n+1} - u_i^{n+1}|_2}{|u_i^{n+1}|_2}$, and $\frac{|p_{i+1}^{n+1} - p_i^{n+1}|_2}{|p_i^{n+1}|_2}$ meets a certain tolerance or the maximum iteration number is reached. Due to an inexact factorization while solving for the linearized system in the Newton-Raphson method, the solution does not always converge to a machine epsilon or a specified small tolerance. When the tolerance is still not reached within the specified number of iterations, the iterations will be stopped by the maximum iteration number criteria. In addition, since Eqs. (17, 19) are solving convective-diffusive equations, high frequency dispersive errors are incurred, unlike when using Eq. (3) in explicit-type schemes. A Nek5000 built-in spectral filter[14] is utilized here for eliminating the high frequency noise in the resolved variables. The Newton-Raphson method is currently implemented in $P_N - P_N$ framework which means that the pressure has the same order of polynomials as the velocity. The instabilities related to a collocated mesh implementation can be cured with the spectral filter[14] as well.

II.D. St. Venant-Kirchhoff solid material

As used in `FSI` benchmark,[16] `St. Venant-Kirchhoff` constitutive law is the extension of a linear elastic material that takes small fintie deformations into consideration.[28] Directly starting from the variational equation of the potential energy integrated over the initial domain, we formulate the problem as: find $d \in H_0^1(\Omega)^d$, such that $\forall w \in H_0^1(\Omega)^d$,

$$\begin{aligned} \delta W &= \delta W^{kin} + \delta W^{int} - \delta W^{ext} \\ &= \int_{\Omega_0} w \cdot \frac{\partial^2 d}{\partial t^2} \rho_0\ d\Omega + \int_{\Omega_0} \frac{\partial W(E)}{\partial E} : \bar{E}(d, w)\ d\Omega - \int_{\Omega_0} w \cdot f\ d\Omega - \int_{\Gamma_0} w \cdot \hat{t}\ d\Gamma. \end{aligned} \tag{21}$$

Here superscripts kin, int, and ext denote kinematic, internal and external energy, respectively. The variables d, ρ_0, f, $\hat{t}$ and Ω_0 are the solid displacement, initial density, body force, traction applied on the initial domain,

and the initial domain itself. Due to St. Venant-Kirchhoff material property, $\frac{\partial W(E)}{\partial E} = S(d) = D : E = \lambda_s tr(E)I + 2\mu_s E$ is the second Piola-Kirchhoff stress associated with Lame's coefficient λ_s, Poisson's ratio μ_s, and $E = \frac{1}{2}(F^T F - I)$ is the Lagrangian strain, $\bar{E}$ is the similar term convolved with test function, $F = I + \nabla_0 d$ is the deformation gradient and operator ∇_0 represents the gradient operated on the initial geometry.

The variational form, Eq. (21), is also nonlinear if expanded in terms of the internal energy term, since stress and strain implicitly depend on the displacement d. To solve it, the `Newton-Raphson` method will still be used for the linearization with the iterative approach, conceptually similar to what was described in Sec. (II.C) but applied to a different non-linear equation. We will then skip the derivation and directly give the increment equation as follows

$$\begin{aligned}(\frac{4M}{\delta t^2} + K)\ \delta d_i^{n+1} &= \int_{\Omega_0} w \cdot f^{n+1}\ d\Omega + \int_{\Gamma_0} w \cdot \hat{t}^{n+1}\ d\Gamma \\ &- \int_{\Omega_0} S(d) : \bar{E}(d, w)\ d\Omega \Big|_i^{n+1} - M[\frac{4}{\delta t^2}(d_i^{n+1} - d^n) + \frac{4}{\delta t}\dot{d}^n - \ddot{d}^n].\end{aligned} \tag{22}$$

Here the mass matrix and stiffness matrix operator are defined as

$$M\ \delta d_i^{n+1} = \int_{\Omega_0} w \cdot \delta d_i^{n+1} \rho_0\ d\Omega, \tag{23}$$

$$\begin{aligned}K\delta d_i^{n+1} &= \int_{\Omega_0} (\delta S : \bar{E} + S : \delta\bar{E})\ d\Omega, \\ \bar{E} &= \frac{1}{2}[\nabla_0 w^T F + (\nabla_0 w^T F)^T], \\ \delta S &= D : \delta E = D : \frac{1}{2}[\nabla_0(\delta d_i^{n+1})^T F + (\nabla_0(\delta d_i^{n+1})^T F)^T], \\ \delta\bar{E} &= \frac{1}{2}[\nabla_0 w^T \nabla_0 \delta d_i^{n+1} + (\nabla_0 w^T \nabla_0 \delta d_i^{n+1})^T].\end{aligned} \tag{24}$$

Eq. (22) could be solved by using `PCG` with the inverse of the mass matrix as the preconditioner. After that, the solid displacement at time step $n+1$ would be updated as

$$d_{i+1}^{n+1} = d_i^{n+1} + \delta d_i^{n+1}. \tag{25}$$

Upon convergence, velocity and acceleration are updated by the Newmark method with a constant average acceleration $\gamma = 0.5,\ \beta = 0.25$ as

$$\begin{aligned}\dot{d}^{n+1} &= \frac{2}{\delta t}(d^{n+1} - d^n) - \dot{d}^n, \\ \ddot{d}^{n+1} &= \frac{4}{\delta t^2}(d^{n+1} - dn) - \frac{4}{\delta t}\dot{d}^n - \ddot{d}^n.\end{aligned} \tag{26}$$

Unlike Eq. (20), only displacement needs to be updated at every iteration, since the current velocity and acceleration are not contained in Eq. (22). Contrary to an inexact factorization employed to solve the fluid equations with the Newton-Raphson method, the increment of the displacement is found here by an exact inverse of the gradient matrix and not approximated, which makes it possible for the solution to be easily converged to machine epsilon for the problems used in our simulations.

II.E. Fluid structure interaction with partitioned coupling

In our implementation, fluid and solid mesh share exactly the same element boundaries at the interface for a perfect matching which obviates the need for interpolation.

The partitioned coupling[7,8,18,29] in a fluid structure interaction problem requires the communication of boundary conditions that are used to enforce the continuity laws across the interfaces. The coupling is usually performed in an iterative manner, involving a certain relaxation method for acceleration of convergence. In the current method, velocity field from the solid on the interface is transferred to a fluid solver and used as a moving mesh boundary condition in the ALE formulation. The sequential algorithm is concluded as follows at time step $n+1$

```
Solve fluid with the interface velocity from solid at previous time step u^n and get traction t_1^{n+1}
Solve solid with the interface traction t_1^{n+1} and get velocity u_1^{n+1}
do loop in i (fsi iteration)
Relaxed the interface velocity u_i^{n+1}
Solve fluid with the relaxed interface velocity u_i^{n+1} and get traction t_i^{n+1}
Solve solid with the interface traction t_i^{n+1} and get velocity u_{i+1}^{n+1}
end loop when converge
Solve fluid one more time with converged velocity u_{i+1}^{n+1}
```

The relaxation method for velocity used here is the Aitken relaxation[7] described as

$$\begin{aligned} u_{i+2}^{n+1} &= (1-\omega_{i+1})u_i^{n+1} + \omega_{i+1}u_{i+1}^{n+1}, \\ \omega_{i+1} &= -\omega_i \frac{R_i \cdot \delta R}{\delta R \cdot \delta R}, \\ R_i &= u_i^{n+1} - u_{i-1}^{n+1}, \\ \delta R &= R_{i+1} - R_i, \\ \omega_1 &= 0.75. \end{aligned} \tag{27}$$

The stopping criteria in the current method is for the normalized L-2 norm of the interface velocity $\frac{|u_{i+1}^{n+1}-u_i^{n+1}|_2}{|u_i^{n+1}|_2}$ to converge to a certain tolerance. Note that the FSI iteration always ends with the fluid solve, in order to provide a better match with the computed solid velocity at the beginning of the next time step.

We note that the fluid mesh is updated by the current mesh velocity solved by an elastic equation with a first order method.[5] However, according to Sec. (II.D), the solid mesh is updated by a second order method which makes the resolved solid velocity $\dot{d}^{n+1}$ of a second order. To avoid any mismatch in geometry, a first order velocity field calculated directly from displacements, $(d^{n+1}-d^n)/\delta t$, would be passed as the boundary condition for the fluid velocity instead of $\dot{d}^{n+1}$ during the FSI coupling.

III. Numerical Results

III.A. Pressure inconsistency in explicit scheme

As mentioned in Sec. (II.A), the drawback of the explicit scheme without sub-iterations lies in an inaccurate extrapolation of the convective term when the surface boundary is moved abruptly. One way to test the response of a numerical scheme to the boundary movement is to manually prescribe a moving pattern of a solid bar and see how the fluid reacts. To be consistent, we use the same geometry and parameters as described in FSI benchmark,[16] and we suddenly apply a non-zero velocity at the bar at time $t \geq 10$.

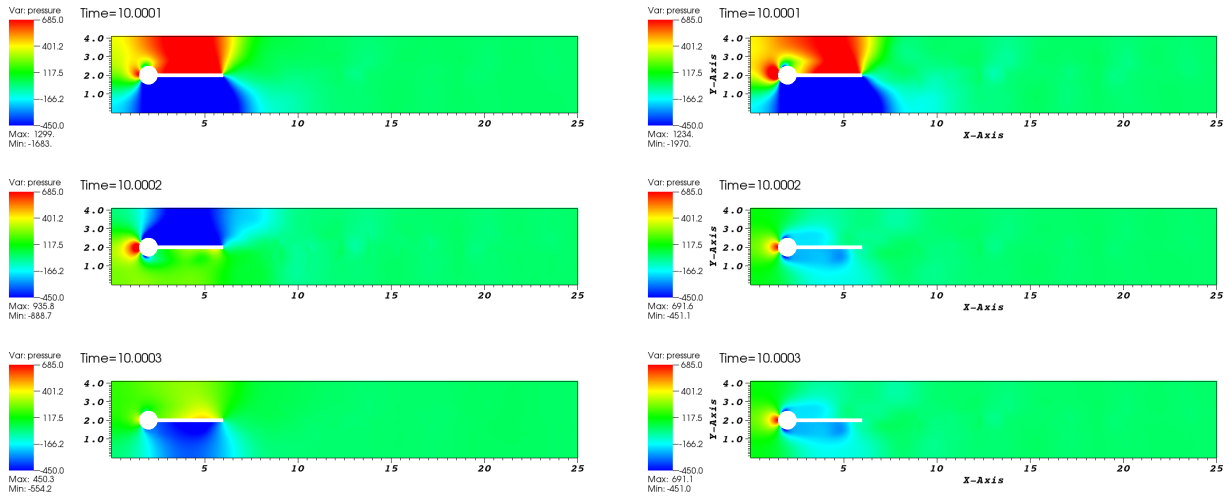

Figure 1. Left: pressure from the explicit scheme for ALE (method II.A.). Right: pressure from the explicit scheme for ALE with the sub-iteration method (method II.B.). A sudden velocity at the bar occurs when $t \geq 10$.

From Fig. 1, it can be told that the pressure from the explicit scheme is not physical for some time after an impulse is applied. It is flipping signs and exhibits sporadic and oscillatory behavior for the first several time steps, however it later stabilizes and shows the same results as with the sub-iteration method. It may not be an issue for a pure fluid problem, with or without the moving boundaries, but it is crucial for an FSI problem since the pressure is directly related to the traction on the solid and, through an interactive feedback loop, it in turn affects the behaviour of the fluid. This results in growing instabilities in the FSI coupling which makes the explicit scheme without sub-iterations to fail.

In what follows, we will be comparing the behavior of different numerical schemes in terms of accuracy and computational performance using an FSI benchmark problem of Turek and Hron.[16] Although the explicit scheme without the sub-iterations will not be used in the FSI coupling for the reasons above, we will still document its comparison with the fluid-only CFD benchmark for completeness.

III.B. FSI benchmark

To validate the fluid-structure interaction solvers, the FSI benchmark[16,30] is commonly used. It is a 2D case that involves an incompressible fluid and a St. Venant-Kirchhoff material. The benchmark geometry in non-dimensional units is demonstrated in Fig. 2, where length scales are normalized with the cylinder diameter D. Boundary conditions consist of a parabolic inflow, constant-pressure derivative-free outflow, and top and bottom no-slip walls. In addition, a stationary solid cylinder is placed inside the domain, with an elastic bar attached to the cylinder. In our geometry, the bar is not strictly rectangular but has a curved side to be fully attached to the cylinder with no gap. When the flow develops, the solid bar reacts to the flow and oscillates. Due to large amplitudes of oscillation in the benchmark problem, it represents a stringent test case to assess both the capability of a smooth mesh construction during the large deformations and the accuracy of the coupled solver.

In order to make sure that the mesh Jacobian stays positive the entire time throughout the duration of the simulations, the variable Young's modulus was empolyed in the elastic mesh deformation solver, with higher stiffness in the regions close to the solid cylinder and the bar, and inversely proportional to the current mesh Jacobian in the rest of the elements.[5]

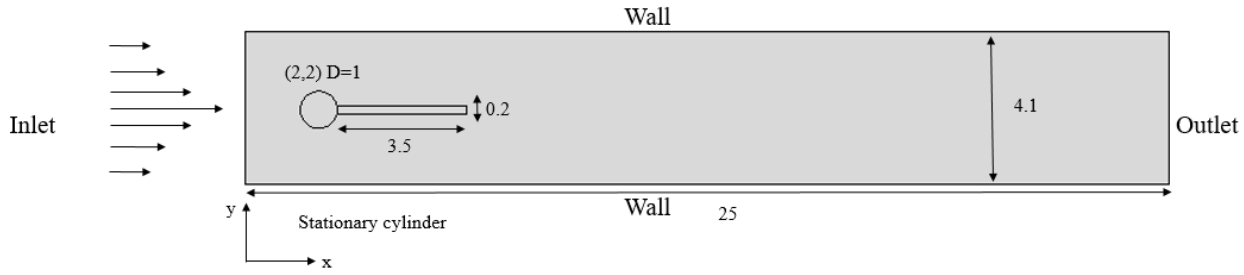

Figure 2. Non-dimensional FSI benchmark geometry

The following inlet profile is used:

$$u_x = \begin{cases} 1.5\,U\,\frac{y(4.1-y)}{(4.1/2)^2}\,\frac{[1-cos(\pi t/2)]}{2} & t \le T \\ 1.5\,U\,\frac{y(4.1-y)}{(4.1/2)^2} & t \ge T, \end{cases}$$

which represents a gradual ramp-up of flow velocity from zero to a desired steady value, with U being a bulk velocity.

The quantities we will compare is the total drag and lift over the solid boundary, which contains the cylinder and the bar, and the displacement of the middle point at the bar tail. There are three test cases for the FSI coupling in the benchmark paper,[30] and also three test cases for the stand-alone fluid and solid solvers as a separate check. In the current paper, we only focus on the third series of test cases, namely `FSI3`, `CFD3` and `CSM3` in Turek and Hron.[16]

The `FSI3` involves the fluid-structure interaction as discussed before. To match the non-dimensional parameters in our simulations with the physical parameters in Turek and Hron,[16] the following non-dimensional values are used: $T = 2$, $U = 20$, density $\rho_f = \rho_s = 1$, fluid viscosity $\mu_f = 0.1$, Young's modulus $E = 560000$, Poisson's ratio $\mu_s = 0.4$, and the reference pressure at outflow $P = 0$.

In `CFD3`, the test case is used to validate the accuracy of the fluid solver only. The geometry remains the same as in `FSI3`, and so do the fluid parameters. However, the solid is set to have no interaction with the fluid and is kept stationary. For the `CFD3` test case, we will again compare the total drag and lift over the solid boundary.

In `CSM3`, the test case is intended to compare the structural behaviour for validating the structure solver. The geometry is still the same, which is a fixed solid cylinder attached to an elastic bar. In this test case, there is a body force (gravity) applied on the solid to initiate the structural motion. Here, we will compare the displacement of the middle point at the bar tail, to see if the solid behaves the same way as in the benchmark. In this case, the geometry is rescaled from the non-dimensional configuration of Fig. 2 back to match the geometry proposed in the benchmark paper.[30] The material properties are as follows: density $\rho_s = 1000$, Poisson's ratio $\mu_s = 0.4$, Young's modulus $E = 1400000$ (different from above), and the gravity acceleration $b_s = 2$.

III.B.1. Solid test case, CSM3

The results are shown in Fig. (3) to document the comparison between our code and the benchmark paper.[30] The time step δt is chosen to be the same as in the later `FSI3` test. The results demonstrate an excellent agreement between the current spectral-element non-linear `St. Venant-Kirchhoff` solid solver and the finite-element benchmark code.

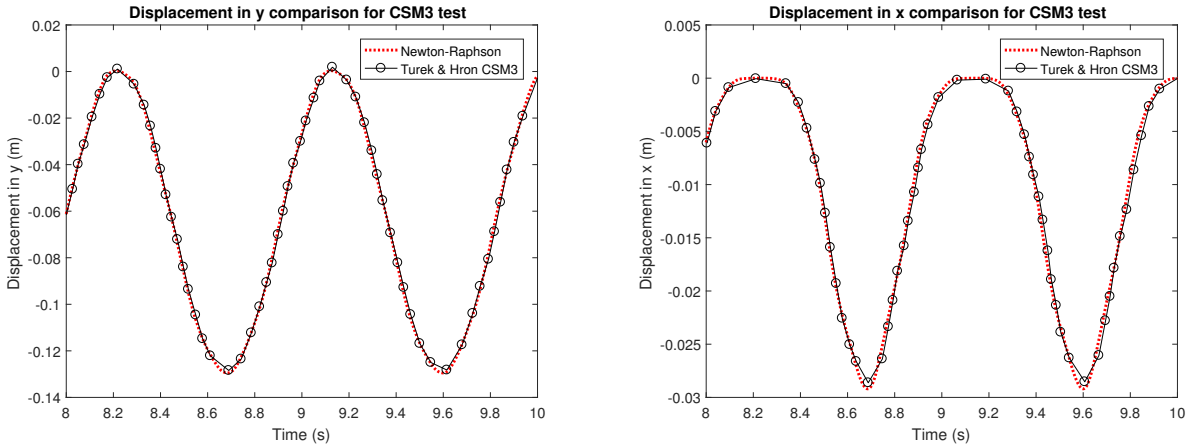

Figure 3. CSM3 test results.

III.B.2. Fluid test case, CFD3

In Fig. (4) we present the lift and drag comparison between the explicit scheme, explicit scheme with sub-iterations, and implicit Newton-Raphson scheme. Identical meshes and the value of time step are used for all the three schemes in this comparison. We observe that both explicit and implicit Newton-Raphson schemes show very good agreement in lift, with the sub-iteration scheme having a very slight discrepancy. We attribute this discrepancy to a slightly lower accuracy of the convective term approximation by sub-iterations as compared to a fully implicit treatment or extrapolation, the latter two being closer to the true value in the current case of *stationary boundary*.

In drag prediction, all three schemes show a slight mismatch with the benchmark indicating a slightly higher value of drag in the current spectral-element simulations. In spite of grid refinement, the drag value of the benchmark could not be matched exactly by any of the schemes, unlike the lift. It could be associated with the way the joint of the cylinder and the bar is treated but it is still yet to be determined.

III.B.3. FSI test case, FSI3

After testing the fluid and the solid part separately, the coupled FSI3 results are presented in Fig. 5. In addition to the values of lift and drag, we also document the x-displacement and the y-displacement of the middle point of the solid bar tail. Unlike in the fluid-only case, the sub-iteration scheme in the full

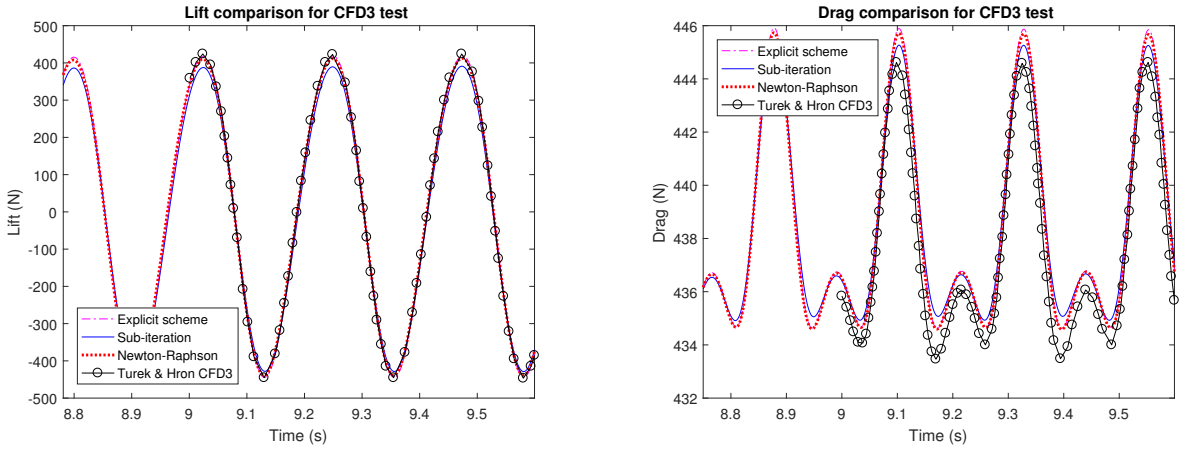

Figure 4. CFD3 test results, results are shifted in time for better comparison.

FSI simulations shows much closer agreement to the benchmark results than the Newton-Raphson scheme. Indeed, the lift and the y-displacement for the sub-iteration scheme match the benchmark values almost perfectly, while the drag and consequently the x-displacement are still very slightly higher. Newton-Raphson scheme, on the other hand, shows a slight disagreement with the benchmark in lift and the y-displacement, and even stronger disagreement in drag and x-displacement. The reason for an inferior accuracy of the Newton-Raphson scheme in the FSI test case in the current implementation might be attributed to the use of filtering for stabilization. Besides of filtering high-frequency noise, the resolved wave numbers may also be affected, the effect potentially amplified in a closed-loop interaction with the elastic solid. Another possible reason is the slow convergence of the fluid solver due to an inexact LU factorization resulting in more frequent termination of the iteration loop by the maximum iteration number criteria rather than the convergence tolerance, especially close to the times when the bar moves to its maximum position corresponding to the largest mesh distortions. One consequence of this effect is that the pressure and the velocity fields are not fully converged resulting in inaccurate traction forces that in turn impact the solid displacements.

III.C. Computational cost

Besides the accuracy, computational cost is important in the FSI simulations since at every time step, it requires a certain amount of iterations between the fluid and the solid solver (FSI iterations), while in the fluid solver, it also requires a certain amount of iterations for using implicit or semi-implicit scheme (fluid iterations). In Fig. 6, a comparison of the iteration counts is presented at a single time step showing how many FSI iterations are needed and, in each FSI iteration, how many sub-iterations or Newton-Raphson iterations are done when the convergence tolerance criteria remains the same between the two schemes.

Apparently, Newton-Raphson method requires more fluid iterations and it also happens to have more FSI iterations. Computational complexity per iteration is also higher for a Newton-Raphson method that requires to solve two vector-valued convective-diffusive equations and one scalar Poisson's equation as opposed to a sub-iteration method that only requires to solve one vector-valued diffusive equation and one scalar Poisson's equation during each iteration. As a result, the CPU time consumption per time step is almost twice as much for the Newton-Raphson method than the sub-iteration method. Combined with the fact that sub-iteration method shows good accuracy in the FSI benchmark comparison, it represents a promising alternative as a fast and accurate method in FSI computations.

IV. Conclusions

In the current paper, three numerical schemes for performing fluid-structure interaction simulations with the spectral-element method Nek5000 were developed and benchmarked: an explicit scheme, an explicit scheme with sub-iterations, and a fully implicit Newton-Rapshon scheme. In a fluid-only comparison with the `CFD3` test, the sub-iteration scheme showed a slight disagreement in lift with the benchmark result with the other two schemes agreeing perfectly, while all the three schemes showed a slight mismatch in drag. It was

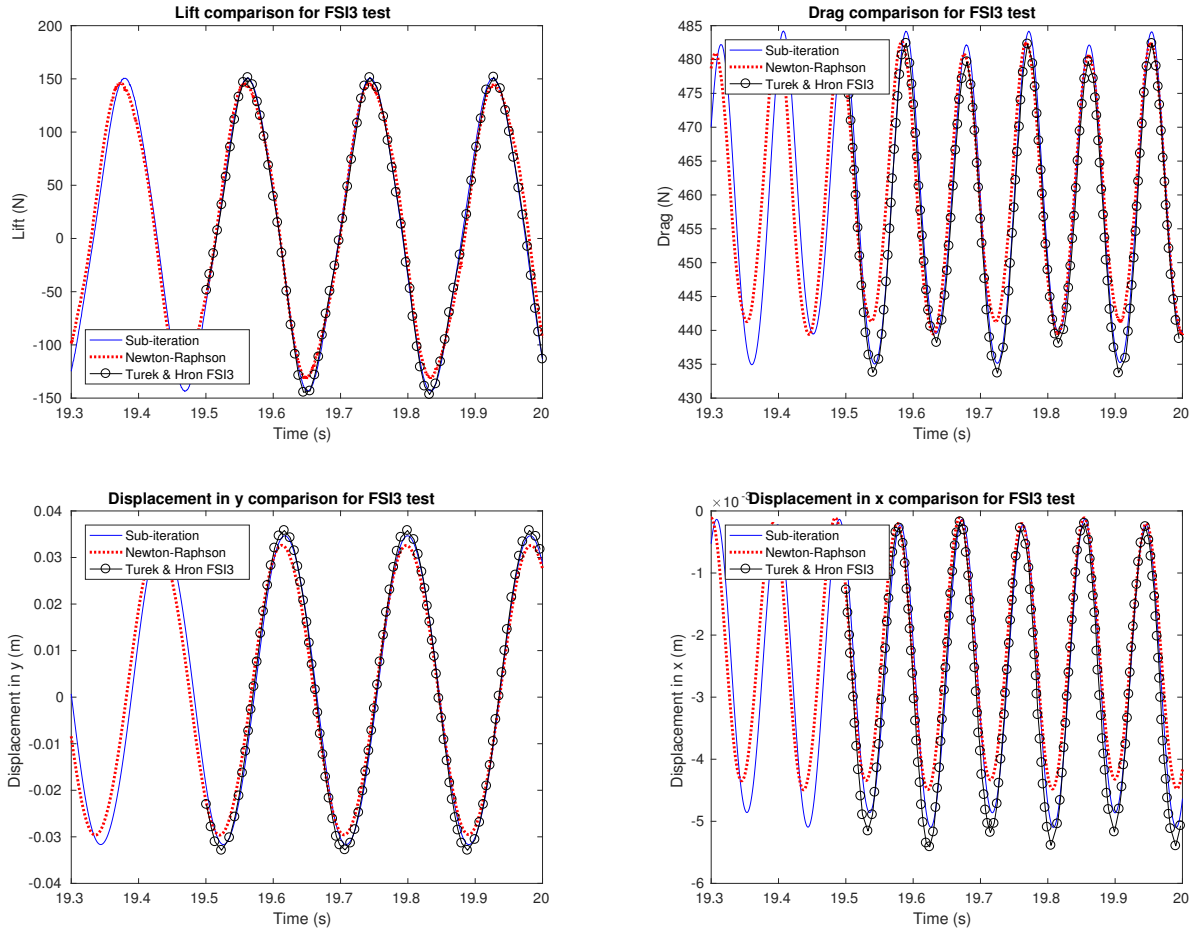

Figure 5. FSI3 test results, results are shifted in time for better comparison.

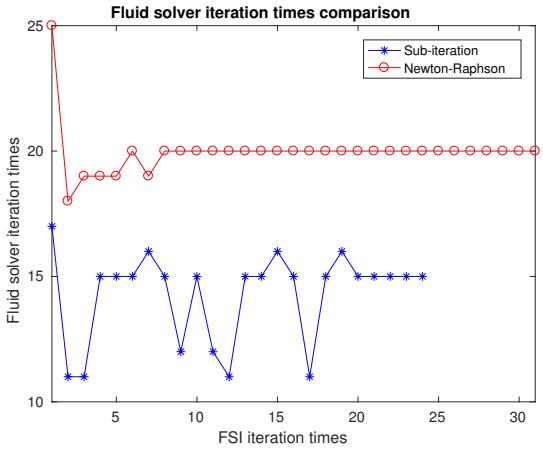

Figure 6. FSI and fluid iteration count comparison at a single time step

further noted that the explicit scheme without sub-iterations is not applicable to fluid-structure interaction simulations due to severe pressure inconsistencies with the rapid mesh motions. It was thus not used in the FSI benchmarking. As for the other two schemes, in the FSI test case `FSI3`, the sub-iteration method surprisingly showed more favorable results in comparison with the Newton-Raphson method, possibly due to an inexact factorization and the slower convergence of the fluid solver in the Newton-Rapshon method

in addition to the use of filtering for stabilization. Combined with the fact that the sub-iteration scheme required significantly less amount of iterations, both in the fluid solver, and in the FSI coupling, and almost double reduction in the computational cost, the explicit sub-iteration scheme can be suggested as a viable candidate for the fluid-structure interaction problems.

References

[1]Michler, C., Hulshoff, S., van Brummelen, H., and deBorst, R., "A monolithic approach to fluid-structure interaction," *Computers & Fluids*, Vol. 33, 2004, pp. 839–848.

[2]Gee, M. W., Küttler, U., and Wall, W. A., "Truly monolithic algebraic multigrid for fluid-structure interaction," *Int. J. Numer. Meth. Engng.*, Vol. 85, 2011, pp. 986–1016.

[3]Heil, M., "An efficient solver for the fully coupled solution of large-displacement fluid-structure interaction problems," *Comput. Methods Appl. Mech. Engrg.*, Vol. 193, 2004, pp. 1–23.

[4]Eken, A. and Sahin, M., "A parallel monolithic algorithm for the numerical simulation of large-scale fluid structure interaction problems," *Int. J. Numer. Meth. Fluids*, Vol. 80, 2016, pp. 687–714.

[5]Bazilevs, Y., Takizawa, K., and Tezduyar, T. E., *Computational Fluid-Structure Interaction Methods and Applications*, A John Wiley & Sons, Ltd, 2013.

[6]Verkaik, A., Hulsen, M., Bogaerds, A., and van de Vosse, F., "An overlapping domain technique coupling spectral and finite elements for fluid-structure interaction," *Computers and Fluids*, Vol. 123, 2015, pp. 235–245.

[7]Küttler, U. and Wall, W., "Fixed-point fluid-structure interaction solvers with dynamic relaxation," *Computational Mechanics*, Vol. 33, 2004, pp. 839–848.

[8]Degroote, J. and Vierendeels, J., "Multi-solver algorithms for the partitioned simulation of fluid-structure interaction," *Comput. Methods Appl. Mech. Engrg.*, Vol. 200, 2011, pp. 2195–2210.

[9]Vierendeels, J., Lanoye, L., Degroote, J., and Verdonck, P., "Implicit coupling of partitioned fluid-structure interaction problems with reduced order models," *Computers and Structures*, Vol. 85, 2007, pp. 970–976.

[10]Förster, C., Wall, W. A., and Ramm, E., "Artificial added mass instabilities in sequential staggered coupling of nonlinear structures and incompressible viscous flows," *Comput. Methods Appl. Mech. Engrg.*, Vol. 196, 2007, pp. 1278–1293.

[11]Razzaq, M., Damanik, H., Hron, J., Ouazzi, A., and Turek, S., "FEM multigrid techniques for fluid-structure interaction with application to hemodynamics," *Applied Numerical Mathematics*, Vol. 62, 2012, pp. 1156–1170.

[12]Chabannes, V., Pena, G., and Prud'homme, C., "High-order fluid-structure interaction in 2D and 3D application to blood flow in arteries," *Journal of Computational and Applied Mathematics*, Vol. 246, 2013, pp. 1–9.

[13]Fischer, P., "An Overlapping Schwarz Method for Spectral Element Solution of the Incompressible NavierStokes Equations," *J. Comp. Phys.*, Vol. 133, 1997, pp. 84–101.

[14]Deville, M. O., Fischer, P. F., and Mund, E. H., *High-Order Methods for Incompressible Fluid FLow*, Cambridge University Press, 2002.

[15]Hughes, T. J. R., *The Finite Element Method: Linear Static and Dynamic Finite Element Analysis*, Dover Publications, 2000.

[16]Turek, S., Hron, J., Razzaq, M., Wobker, H., and Schäfer, M., "Numerical Benchmarking of Fluid-Structure Interaction: A comparison of different discretization and solution approaches," *Fluid Structure Interaction II*, Vol. 73, 2010, pp. 413–424.

[17]Hirt, C. W., Amsden, A. A., and Cook, J. L., "An arbitrary LagrangianEulerian computing method for all flow speeds," *Journal of Computational Physics*, Vol. 14, 1974, pp. 227–253.

[18]Baek, H., *A Spectral Element Method for Fluid-Structure Interaction:New Algorithm and Applications to Intracranial Aneurysms*, Ph.D. thesis, Brown University, Providence, May 2010.

[19]Newmark, N. M., "A method of computation for structured dynamics," *Journal of Engineering Mechanics,ASCE*, Vol. 85, 1959, pp. 67–94.

[20]Bernardi, C. and Maday, Y., "Uniform inf-sup conditions for the spectral discretization of the Stokes problem," *Math. Models Methods Appl. Sci*, Vol. 9(3), 1999, pp. 395–414.

[21]Merrill, B. E., *High-Order Moving Overlapping Grid Methodology in a Spectral Element Method*, Ph.D. thesis, Arizona State University, Tempe, 2015.

[22]Kirby, R. M., Yosibash, Z., and Karniadakis, G. E., "Towards stable coupling methods for high-order discretization of fluid-structure interaction: Algorithms and observations," *Journal of Computational Physics*, Vol. 223, 2007, pp. 489–518.

[23]Baek, H. and Karniadakis, G. E., "Sub-iteration leads to accuracy and stability enhancements of semi-implicit schemes for the NavierStokes equations," *Journal of Computational Physics*, Vol. 230, 2011, pp. 4384–4402.

[24]Pena, G., Prudhomme, C., and Quarteroni, A., "High order methods for the approximation of the incompressible Navier-Stokes equations in a moving domain," *Comput. Methods Appl. Mech. Engrg.*, Vol. 209–212, 2012, pp. 197–211.

[25]Gervasio, P., Saleri, F., and Veneziani, A., "Algebraic fractional-step schemes with spectral methods for the incompressible NavierStokes equations," *Journal of Computational Physics*, Vol. 214, 2006, pp. 347–365.

[26]Gervasio, P., "Convergence Analysis of High Order Algebraic Fractional Step Schemes for Time-Dependent Stokes Equations," *SIAM J. NUMER. ANAL*, Vol. 46(4), 2007, pp. 1682–1703.

[27]Quarteroni, A., Saleri, F., and Veneziani, A., "Analysis of the Yosida method for the Incompressible Navier?Stokes equations,," *J. Math. Pures Appl*, Vol. 78(5), 1999, pp. 473–503.

[28]Kim, N.-H., *Introduction to Nonlinear Finite Element Analysis*, Springer, 2002.

[29]Matthies, H. G. and Steindorf, J., "Partitioned strong coupling algorithms for fluid-structure interaction," *Computers and Structures*, Vol. 81, 2003, pp. 805–812.

[30]Turek, S. and Hron, J., "Proposal for Numerical Benchmarking of Fluid-Structure Interaction between an Elastic Object and Laminar Incompressible Flow," *Fluid-Structure Interaction*, Vol. 53, pp. 371–385.